

Article

Rate Dependence of the Compressive Response of Ti Foams

Petros Siegkas ^{1,*}, Vito L. Tagarielli ², Nik Petrinic ¹ and Louis-Philippe Lefebvre ³

¹ Department of Engineering Science, University of Oxford, Parks Road, Oxford OX13PJ, UK; E-Mail: nik.petrinic@eng.ox.ac.uk

² Department of Aeronautics, Imperial College London, South Kensington Campus, London SW72AZ, UK; E-Mail: v.tagarielli@imperial.ac.uk

³ NRC Canada, Industrial Materials Institute, 75 de Mortagne, Boucherville QC J4B6Y4, Canada; E-Mail: louis-philippe.lefebvre@imi.cnrc-nrc.gc.ca

* Author to whom correspondence should be addressed; E-Mail: petros.siegkas@worc.ox.ac.uk; Tel.: +4-474-274-917-05.

Received: 27 April 2012; in revised form: 22 May 2012 / Accepted: 20 June 2012 /

Published: 29 June 2012

Abstract: Titanium foams of relative density ranging from 0.3 to 0.9 were produced by titanium powder sintering procedures and tested in uniaxial compression at strain rates ranging from 0.01 to 2,000 s⁻¹. The material microstructure was examined by X-ray tomography and Scanning Electron Microscopy (SEM) observations. The foams investigated are strain rate sensitive, with both the yield stress and the strain hardening increasing with applied strain rate, and the strain rate sensitivity is more pronounced in foams of lower relative density. Finite element simulations were conducted modelling explicitly the material's microstructure at the micron level, via a 3D Voronoi tessellation. Low and high strain rate simulations were conducted in order to predict the material's compressive response, employing both rate-dependant and rate-independent constitutive models. Results from numerical analyses suggest that the primary source of rate sensitivity is represented by the intrinsic sensitivity of the foam's parent material.

Keywords: titanium foams; FE; Voronoi; X-ray tomography; strain rate

1. Introduction

Titanium and its alloys can be characterized by pronounced strain hardening [1] and possess good impact resistance due to their strain rate sensitivity [2]. Powder sintering routes allow production of cellular solids [3] made from Ti and Ti alloys [4,5]. These materials are of interest to the aerospace and defence industry due to their good dynamic specific energy absorption, and attract the attention of the bio-medical industry due to good mechanical properties combined with biocompatibility. While the static and dynamic mechanical response of Ti and Ti alloys have been thoroughly investigated (see for example [6–8]), less work exists on the response of Ti and Ti alloy foams. Several authors conducted quasi-static compression, tension and bending tests experiments on open-cell and closed-cell [9–11] Ti foams manufactured by the space-holder method, which consists in compacting and sintering a mixture of Ti powder and a polymeric space-holder in order to obtain pores of controllable size. Experiments revealed that the foams can be anisotropic, and that their mechanical properties can be tuned to be similar to those of cancellous and cortical bone by varying the relative density. Tuncer and Arslan [12] tested in compression Ti foams of relative density $\bar{\rho} = 0.3–0.8$, produced by optimizing the space-holder method. The materials were deformed at low and medium strain rates ($10^{-3}–6 \times 10^{-6}$) and were found to be mildly strain rate sensitive in this range. Thelen *et al.* [13] worked with sintered foams obtained from both commercially pure Ti and TiAl6V4 powders, of relative densities in the range of $\bar{\rho} = 0.2–0.5$. Specimens were subjected to quasi-static mechanical loading in order to determine their elastic properties, and found them in good agreement with the predictions of Mori and Tanaka [14] and Ashby and Gibson [15]. The fragmented existing experimental studies [12] suggest that Ti foams can be mildly sensitive to strain rate in compression. This is in contrast with the results reported by other authors on lower-density Al foams [16,17], which show a rate-insensitive response. In this study, we focus on the compressive properties of pure Ti foams produced using a powder metallurgy process [18] and the measured responses are compared with those of Ti powder sintered under similar conditions to the foams. In order to understand the dependence of the material response on relative density and strain rate, foams with $\bar{\rho} = 0.3–0.93$ are tested in compression at strain rates from 0.01 to 2,000 s^{-1} .

Several authors have addressed the mechanical response of cellular solids via FE simulations. Shen *et al.* [19] modeled the microstructure of foams of relative density up to 0.15 by introducing spherical pores in a homogeneous matrix, and found simulations in reasonable agreement with experimental data. Such an approach is not suitable for the high-density foams investigated here, due to the fact that these foams have pores of irregular shape and pore internal surfaces experience self contact during compressive deformation. Borovinsek *et al.* [20] modeled the microstructure of high porosity lattice structures via 3D Voronoi tessellations. The foams were subjected to quasi static and dynamic loading and the effect of irregularity to the material response was studied; on the other hand, results were not compared to experimental evidence.

In this paper we shall use 3D Voronoi tessellations to reproduce the microstructure of sintered Ti foams of relative density 0.3–0.9; FE predictions will be employed to understand the nature of the material's strain rate sensitivity.

2. Experimental Procedures and Results

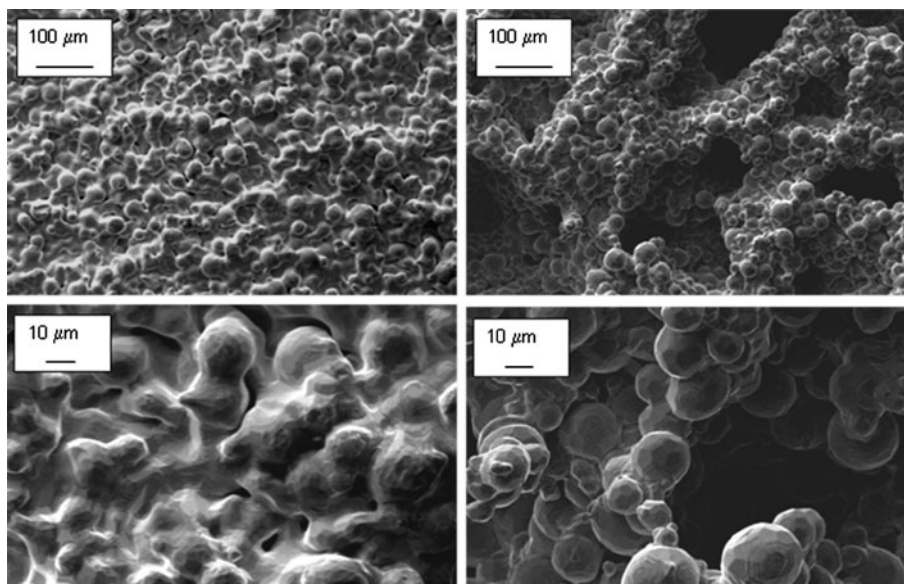
2.1. Material Manufacturing

Sintered Ti powders and foams were produced from 99.9% purity Titanium using the process described in [18]. Briefly, titanium powder was mixed with a binder and a chemical foaming agent. The resulting mixture was poured into a mould and heated in order to foster the foaming process; subsequently, the material was de-binded and sintered. During foaming the binder melts and forms a suspension with the Ti particles. The foaming agent then decomposes and generates a gas that expands the suspensions; after foaming, the binder is eliminated by thermal decomposition. Specimens with different porosity levels are produced by modifying the composition of the mixture. The resulting material is cut into circular cylindrical specimens which are then sintered at high temperature to consolidate the material. In order to understand the material response in absence of porosity, sintered Ti powder specimens were produced by a similar route to that described above, absent the foaming agent and the binder.

2.2. Geometrical Analysis of the Foam Microstructure

Scanning Electron Microscopy (SEM) and X-ray micro tomography were used to examine the microstructure of the foams and to measure pore size distribution. It was observed that the material was made from an assembly of sintered powder particles of polyhedral shape. Two levels of porosity were visible in the material: (1) a macro-porosity which results from the foaming process; (2) a micro-porosity resulting from incomplete sintering of the Ti powder (Figure 1). For the foam of highest density ($\bar{\rho} = 0.91$), produced by powder sintering with the foaming agent absent, powder particles are nearly completely sintered and only small micro-voids are observed, of diameter around 10 μm . Foams of low relative density ($\bar{\rho} = 0.45$), display larger macro-voids of diameter ranging from 100 to 300 μm ; the degree of sintering is lower for these foams compared with that of high-density foams.

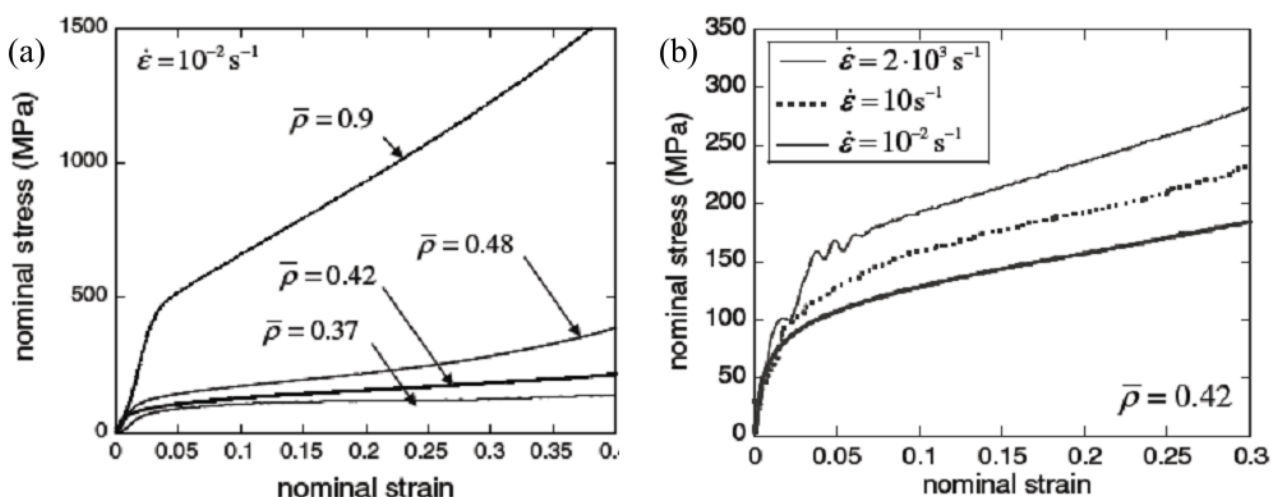
Figure 1. Scanning Electron Microscopy (SEM) images of high relative density ($\bar{\rho} = 0.91$, **left**) and low-density ($\bar{\rho} = 0.45$, **right**) foams.



2.3. Quasi-Static Uniaxial Compression Experiments

Foams of densities $\bar{\rho} = 0.3-0.9$ were tested in uniaxial compression at strain rates of 0.01 s^{-1} . Circular cylindrical specimens of diameter 11 mm and height of 13 mm were compressed in the axial direction. A screw driven machine in displacement control was used to conduct the experiments. The compressive force was measured by a resistive load cell, and the shortening of the sample was measured by a laser extensometer and was used to calculate the compressive strain. Experiments were interrupted when an axial strain larger than 0.5 was achieved. Figure 2a presents the measured stress *versus* strain curves for samples of four different densities. Image correlation was used to measure transverse deformation of the sample; the ratio of this transverse strain to the imposed compressive axial strain is defined as the material Poisson's ratio. Tests showed the elastic modulus scales with relative density according to a power-law of exponent 1.08 which is approximately half of that predicted by Ashby *et al.* [15] for low density polymeric foams.

Figure 2. (a) Quasi-static compressive response of Ti foams of different densities; (b) Effect of strain rate on the compressive response of a Ti foam of relative density $\bar{\rho} = 0.42$.



2.4. Dynamic Compression Experiments

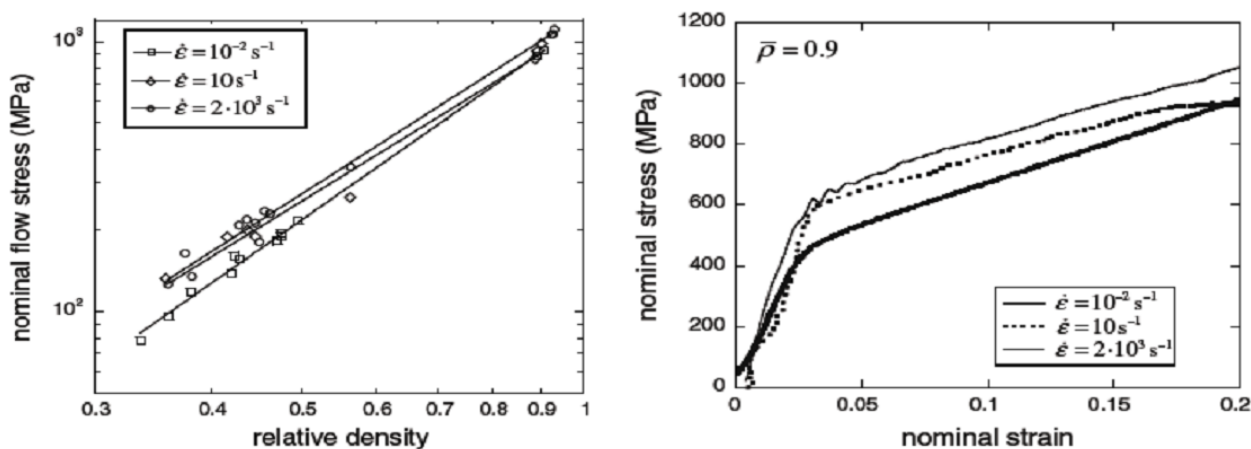
In order to measure the dependence of the material response upon the rate of strain, dynamic uniaxial compression tests were performed on circular cylindrical samples of diameter 11 mm and height 5 mm.

Medium Rate Experiments: A hydraulic machine was used to load the sample. A light steel piston compressed the foam specimens at velocities of the order of 0.05 ms^{-1} , corresponding to imposed strain rates of the order of 10 s^{-1} . High-speed photography was employed to measure strains.

High Rate: In order to achieve a strain rate of the order of $1,000 \text{ s}^{-1}$, a split pressure Hopkinson bar (SPHB) setup was used [21], with all bars made from hardened steel and strain gauges attached on the input and output bars. The sample shortening was obtained via both stress wave analysis and high-speed photography. Force equilibrium was typically reached after $10 \mu\text{s}$, corresponding to an axial strain around 0.03, and the imposed strain rate was approximately constant after this time. Figure 2b presents a comparison of the stress *versus* strain response for a foam of density $\bar{\rho} = 0.42$ at different strain rates.

Due to the limited size of the specimens in comparison to microstructural features, scatter was significant. This is shown in Figure 3 (left), which presents the variation of the flow stress (at a plastic strain of 0.2) as a function of density and strain rate. At each strain rate, the yield stress scales with foam density according to a power-law with exponent and intercept depending on the imposed strain rate. Figure 3 also displays the measured stress *versus* strain response of sintered Ti powder, of relative density 0.9; the data shows that the material's yield point increases with imposed strain rate while the strain hardening rate is approximately insensitive to speed of deformation.

Figure 3. (Left) Measured flow stress (at a plastic strain of 0.2) as a function of foam density and strain rate; (Right) Stress *versus* strain response of sintered powder of relative density $\bar{\rho} = 0.9$ at low, medium and high strain rates.



2.5. FE Simulations of the Compressive Response

Abaqus was employed to perform static and dynamic simulations of the foams response. The microstructure of the foams was reproduced using a random 3D Voronoi tessellation [22] of the specimen's space. A cube of material was subdivided in randomly-shaped Voronoi cells and a number of these cells was flagged as pores. The density of the seed points was chosen in order to ensure that the distribution of pore sizes followed that measured via X-ray tomography. The solid material defined by the difference between the specimen domain and the pore domains was meshed with linear tetrahedral and hexahedral elements by a commercial meshing tool [23]. The representative volume element for the geometrical characteristics was defined as the minimum volume that can include a set of pores with size (cubic root of pore volume) characterized by a probability distribution approximately equal to that measured via X-ray tomography.

Compressive loading was applied by imposing a displacement on the top and bottom faces of the mesh. Periodic boundary conditions were applied on lateral faces, imposing that opposite lateral faces moved by a uniform displacements, perpendicular to the faces and of equal and opposite amount. J_2 incremental plasticity was used to model deformation of the foams parent material, and the strain hardening was chosen to be isotropic and was calibrated against the data for the sintered powders of density 0.9 shown in Figure 3 (right). Both rate-sensitive and rate-insensitive models were used. The rate sensitivity was described by a power-law dependence of the flow stress upon the applied strain rate, and was deduced from the compressive stress *versus* strain curves obtained by testing the parent

material at different strain rates; the exponent of the power-law expression (of type $\sigma_{0.2} = A\dot{\epsilon}^m$) was found to be 0.016. Figures 4 and 5 display samples of the mesh and the FE predictions of the macroscopic compressive response at low ($\sim 0.01/s$) and high ($\sim 1,000/s$) strain rate, for foams of two selected densities. By comparing with the data in Figure 3 (left), it is evident that the FE simulations predict accurately the yield stress for these foams.

Figure 4. (Left) mesh of a virtual foam of relative density $\bar{\rho} = 0.49$; **(Right)** FE predictions of the macroscopic material responses.

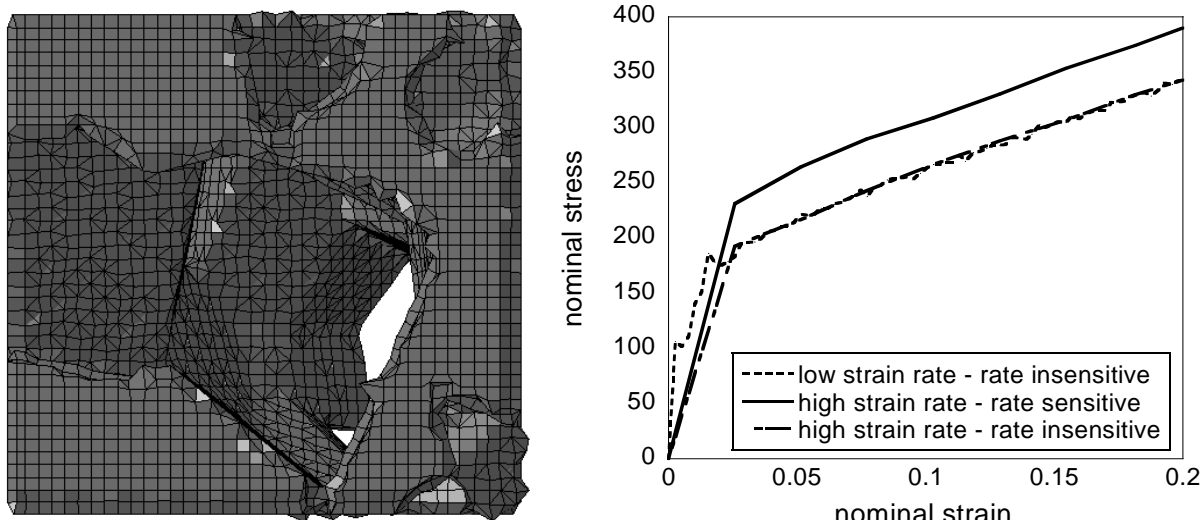
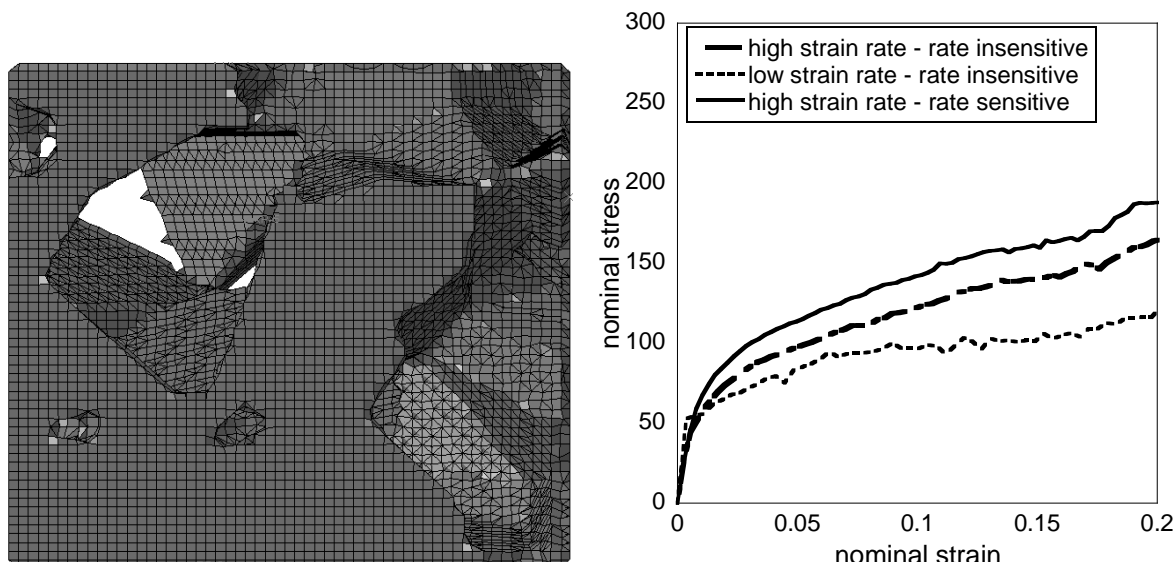


Figure 5. (Left) mesh of a virtual foam of relative density $\bar{\rho} = 0.36$; **(Right)** FE predictions of the macroscopic material responses.



3. Discussion

At all compressive strain rates, foams initially deform elastically and subsequently collapse plastically by flattening of the macro-pores perpendicularly to the loading direction. Correspondingly, strain hardening is observed in the macroscopic response, due to progressive self-contact of the internal

surfaces of the pores. A separate set of simulations, conducted employing a perfectly plastic response, confirmed that the predicted macroscopic strain hardening is due partially to pore self-contact and partially to the intrinsic strain hardening characteristic of the parent material. At compressive axial strains in the range 0.15–0.3, micro-cracking is observed. At sufficiently high axial strains the strain hardening rate increases for these foams, due to material densification by complete closure of the pores (densification).

The static and dynamic mechanical response of the foams is sensitive to relative density; elastic modulus, flow stress and strain hardening rate increase with the foam relative density. Comparisons of the measured stress–strain responses at different strain rates revealed that the material response is sensitive to the applied strain rate. Sintered Ti powder ($\bar{\rho} = 0.9$) displays an increase of the yield stress with strain rate comparable to those observed by other authors [6–8] for fully dense crystalline Ti alloys. This elevation in yield stress was measured to be of 13% as the strain rate was varied from 0.01 to 2,000 s⁻¹; for these sintered powders, the measured strain hardening rate is independent of the applied strain rates. Foams ($\bar{\rho} = 0.3–0.5$) display an elevation of both yield stress and strain hardening rate with increasing applied strain rate. Foams with relative density $\bar{\rho} = 0.33$ displayed an elevation of 32% in flow stress (at a plastic strain of 0.2) as the strain rate was varied from 0.01 to 2,000 s⁻¹. In more quantitative terms, the measured flow stress (at a plastic strain of 0.2) $\sigma_{0.2}$ versus imposed strain rate ($\dot{\epsilon}$) data could be fitted by a power-law relation of type $\sigma_{0.2} = A\dot{\epsilon}^m$, where A and m were a function of relative density. The measured exponents m were found to be 0.027 and 0.017 for relative densities of 0.35 and 0.9, respectively.

FE predictions help understanding of the origin of strain rate sensitivity. Figure 4 shows that for foams of relatively high density the low and high strain rate macroscopic responses coincide in the case where intrinsic rate sensitivity of the parent material is not modelled. We deduce that the effects of micro-inertia are negligible for foams of this density. In contrast, for foams of lower density, such as that associated to the mesh and data in Figure 5, the FE-predicted high strain rate response is stronger than the low strain rate response in absence of rate sensitivity of the parent material. Modelling such sensitivity gives an even stronger macroscopic high strain rate response. We deduce that for foams of lower density micro-inertial effects contribute positively to the macroscopic rate sensitivity of the material.

4. Conclusions

The Ti foams under investigation displayed strain rate sensitivity, with both yield stress and strain hardening rate increased with increasing strain rate. Strain rate sensitivity appears to be more pronounced for foams of lower relative density: numerical analyses suggest that the primary source of rate sensitivity is represented by the intrinsic sensitivity of the sintered powders, however micro-inertial effects intervene for rapid loading of foams of lower relative density.

Acknowledgments

The Authors acknowledge financial support from the Department of Engineering Science and Worcester college at Oxford University and also the National Research Council Canada (Industrial Materials Institute, material manufacturing) for providing specimen material.

References

1. Long, M.; Rack, H.J. Titanium alloys in total joint replacement—A material science perspective. *Biomaterials* **1998**, *19*, 1621–1639.
2. Nemat-Nasser, S.; Guo, W.G.; Cheng, J.Y. Mechanical properties and deformation mechanisms of commercially pure Titanium. *Acta Mater.* **1999**, *47*, 3705–3720.
3. Ashby, M.F.; Evans, A.G.; Fleck, N.A.; Hutchinson, J.W.; Wadley, H.N.G.; Gibson, L.J. Making metal foams. In *Metal Foams: A Design Guide*; Butterworth-Heinemann: Burlington, MA, USA, 2000.
4. Lefebvre, L.P.; Baril, E.; Bureau, M.N. Effect of the oxygen content in solution on the static and cyclic deformation of titanium foams. *J. Mater. Sci. Mater. Med.* **2009**, *20*, 2223–2233.
5. Jorgensen, D.J.; Dunand, D.C. Ti-6Al-4V with micro- and macropores produced by powder sintering and electrochemical dissolution of steel wires. *Mater. Sci. Eng. A* **2010**, *527*, 849–853.
6. Guden, M.; Celik, E.; Akar, E.; Cetiner, S. Compression testing of a sintered Ti6Al4V powder compact for biomedical applications. *Mater. Char.* **2005**, *54*, 399–408.
7. Rouxel, A.; Chiem, C.Y. Strain-rate history effects on TiAl6V4 titanium alloy. *Impact Loading Dynam. Behav. Mater.* **1988**, *2*, 601–608.
8. Meyer, L.W.; Krüger, L.; Razorenov, S.V.; Kanel, G.I. Investigation of dynamic flow and strength properties of Ti-6-22-22S at normal and elevated temperatures. *In. J. Impact Eng.* **2003**, *28*, 877–890.
9. Wen, C.E.; Yamada, Y.; Shimojima, K.; Chino, Y.; Asahina, T.; Mabuchi, M. Processing and mechanical properties of autogenous titanium implant materials. *J. Mater. Sci. Mater. Med.* **2002**, *13*, 397–401.
10. Wen, C.E.; Mabuchi, M.; Yamada, Y.; Shimojima, K.; Chino, Y.; Asahina, T. Processing of biocompatible porous Ti and Mg. *Scr. Mater.* **2001**, *45*, 1147–1153.
11. Imwinkelried, T. Mechanical properties of open-pore titanium foam. *J. Biomed. Mater. Res. A* **2007**, *81A*, 964–970.
12. Tuncer, N.; Arslan, G. Designing compressive properties of titanium foams. *J. Mater. Sci.* **2009**, *44*, 1477–1484.
13. Thelen, S.; Barthelat, F.; Brinson, L.C. Mechanics considerations for microporous titanium as an orthopedic implant material. *J. Biomed. Mater. Res.* **2004**, *69A*, 601–610.
14. Mori, T.; Tanaka, K. Average stress in matrix and average elastic energy of materials with misfitting inclusions. *Acta Metall.* **1973**, *21*, 571–574.
15. Ashby, M.F.; Gibson, L.J. Mechanics of foams. In *Cellular Solids: Structure and Properties*; Cambridge University Press: New York, NY, USA, 1997.
16. Deshpande, V.S.; Fleck, N.A. Isotropic constitutive models for metallic foams. *J. Mech. Phys. Solid.* **2000**, *48*, 1253–1283.
17. Radford, D.D.; Deshpande, V.S.; Fleck, N.A. The use of metal foam projectile to simulate shock loading on a structure. *Int. J. Impact Eng.* **2005**, *31*, 1152–1171.
18. Lefebvre, L.P.; Thomas, Y. Method of Making Open Cell Material. U.S. Patent 6,660,224, 9 December 2003.

19. Shen, H.; Oppenheimer, S.M.; Dunand, D.C.; Brinson, L.C. Numerical modeling of pore size and distribution in foamed titanium. *Mech. Mater.* **2006**, *38*, 933–944.
20. Borovinsek, M.; Ren, Z. Computational modelling of irregular open-cell foam under impact loading. *Mater. Sci. Eng. Technol.* **2008**, *39*, 114–120.
21. Gray, G.T. *Classic Split Hopkinson Pressure Bar Testing*; ASM International: Materials Park, OH, USA, 2000; pp. 462–476
22. Georgy Voronoi. Nouvelles applications des paramètres continus à la théorie des formes quadratiques. *J. Pure Appl. Math.* **1908**, *133*, 97–178
23. *Beta CAE Systems S.A. Ansa v. 12.1.3 User's Guide*; Makedonia Palace: Thessaloniki, Greece, 2008; Chapter 10, Volume Meshing, pp. 503–575.
24. Abaqus Analysis User's Manual, Classical Metal Plasticity, Rate Dependence-Direct Tabular Data. Simulia Abaqus CAE 6.9 Documentation, Maastricht, The Netherlands, 2009.

© 2012 by the authors; licensee MDPI, Basel, Switzerland. This article is an open access article distributed under the terms and conditions of the Creative Commons Attribution license (<http://creativecommons.org/licenses/by/3.0/>).